JACS
JOURNAL OF THE AMERICAN CHEMICAL SOCIETY

ARTICLE

pubs.acs.org/JACS

Identification of the Active Species Generated from Supported Pd Catalysts in Heck Reactions: An in situ Quick Scanning EXAFS Investigation

Sven Reimann,[†] Jan Stötzel,[‡] Ronald Frahm,[‡] Wolfgang Kleist,[†,§] Jan-Dierk Grunwaldt,[*,§,⊥] and Alfons Baiker[*,†]

[†]Institute for Chemical and Bioengineering, Department of Chemistry and Applied Biosciences, ETH Zurich, Hönggerberg, HCI, CH-8093 Zurich, Switzerland

[‡]Department C - Physics, University of Wuppertal, Gausstrasse 20, D-42097 Wuppertal, Germany

[§]Institute for Catalysis Research and Technology (IKFT), Karlsruhe Institute of Technology (KIT), Herrmann-von-Helmholtz-Platz 1, D-76344 Eggenstein-Leopoldshafen, Germany

[⊥]Institute for Chemical Technology and Polymer Chemistry (ITCP), Karlsruhe Institute of Technology (KIT), Kaiserstr. 12, D-76128 Karlsruhe, Germany

Supporting Information

ABSTRACT: Quick scanning extended X-ray absorption fine structure (QEXAFS) studies in the subsecond time scale have been performed to gain insight into the reaction mechanism of Heck-type C−C coupling reactions in the presence of supported Pd-based catalysts. Using a specially designed in situ EXAFS cell, both the solid catalyst and the liquid reaction mixture during the reaction of phenyl bromide (PhBr) with styrene were monitored. Soluble Pd species were only, but rapidly, detected in the liquid reaction phase once the reaction temperature of 150 °C was reached. At the same time, the conversion of PhBr started, and during the following "active phase" of the catalyst hardly any changes in the corresponding EXAFS and XANES spectra were observed. The present species could be identified as colloidal Pd^0 clusters with a size of ∼2 nm estimated from the corresponding EXAFS spectra. The QEXAFS mode not only allowed monitoring rapid changes in the second time scale but also permitted minimization of effects caused by the heterogeneity of the systems. When the reaction rate started to decrease, pronounced changes in the EXAFS spectra were observed, which were attributed to an increased formation of bromo-palladates ($[PdBr_4]^{2-}$, $[Pd_2Br_6]^{2-}$). In addition to the liquid-phase species, significant changes were observed for the solid catalyst that was also probed in situ during the reaction. The originally oxidized Pd catalyst was efficiently reduced upon heating. Additionally, growth of the supported Pd particles was observed by both EXAFS and STEM. The above results confirm the role of the soluble molecular Pd species as the catalytically active species and clarify their conjunction with the in situ formed Pd colloids. Furthermore, the investigation demonstrates the potential of the QEXAFS not only for monitoring rapid changes during catalysis but also for gaining deeper insight into the mechanism of such complex industrially important systems under relevant reaction conditions.

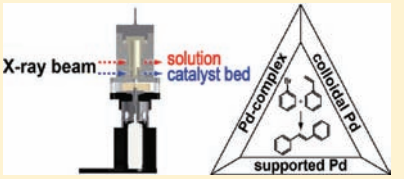

INTRODUCTION

C−C coupling reactions are a versatile tool in synthetic chemistry and are of practical interest in industry.[1,2] One of the most thoroughly investigated is the Heck coupling reaction (Scheme 1).[3−5] It is usually catalyzed by homogeneous Pd complexes, often with phosphine ligands, in the presence of a base. The advantage of this reaction is its high tolerance to a wide range of functional groups and the good availability of aryl bromides and chlorides.[5] However, from a practical point of view, heterogeneous catalysts are often preferred to homogeneous ones because of their easier handling. Nonetheless, one may be confronted with other challenges in the case of heterogeneous catalysts. Besides the generally lower activity and selectivity compared to their homogeneous counterparts, they may only serve as precursors for an in situ formed homogeneous catalyst.

In particular, the reaction mechanism of the heterogeneously catalyzed, ligandless Heck coupling reaction is still a matter of discussion and speculation. One of the most popular mechanisms describes a reaction pathway where the palladium is leached into the liquid phase from a heterogeneous precursor or from Pd colloids that were intermediately formed from organometallic precursors.[6−8] Consequently, the active species is suggested to be a homogeneous complex formed in situ from the leached Pd.

Received: September 24, 2010
Published: February 23, 2011

Scheme 1. Heck Coupling of PhBr (1) with Styrene (2), Leading to the Formation of *trans*-Stilbene (3), *cis*-Stilbene (4), Diphenylethylene (5), and Diphenyl (6)

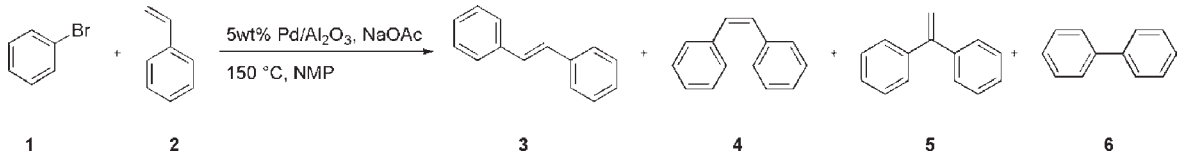

In contrast, mechanisms assuming a purely heterogeneously catalyzed Heck coupling have been suggested as well.[9,10] Depending on the reaction conditions, the formation of Pd colloids and/or the redeposition of the Pd on a support can be observed, and a lot of effort has been put into the control of this behavior in the past. However, it is difficult to detect intermediate palladium species and their dynamic behavior during the reaction based on ex situ methods such as transmission electron microscopy (TEM), ESI-MS, ICP-MS, or ICP-OES, which can only give a snapshot of the reaction mixture.[11,12] In addition, it has been shown that very small concentrations of the catalytically active species in solution are sufficient to catalyze the reaction but might be difficult to detect using these techniques.[13] In contrast, spectroscopic in situ investigations allow following the operation and changes of a catalyst in real time and thus provide crucial information about the structural changes of the catalyst.[14] Nevertheless, only a few studies dealing with such in situ investigations for C−C coupling reactions have been published to date.[15−17]

EXAFS is a promising in situ technique in this case because it allows selectively monitoring the Pd-containing species and additionally resolving their specific structure.[14,15,18,19] It is further possible to study very small particles and species with short-range order in solution, which are decisive advantages compared to other structure-resolving techniques like e.g. XRD and NMR. Since changes in such reactions may happen in a quite short time frame, the Quick EXAFS (QEXAFS) technique was used to monitor the reaction.[20−24] Here, a time-resolved investigation on the subsecond scale was achieved, while maintaining all the mentioned advantages of the EXAFS technique. In addition, new tools for QEXAFS data analysis are presented and applied to the data to meet the challenges of this experiment, namely the low concentrations of Pd species and the complex mixtures of them. With a combination of EXAFS and XANES analysis techniques, the maximum of information was extracted from the data. To investigate the leaching behavior, a special cell with two beam paths for the X-ray beam was used, which allows probing the catalyst bed and the liquid phase separately.[25]

EXPERIMENTAL SECTION

Materials. Phenyl bromide (**1**, PhBr, Fluka, >99.5%), styrene (**2**, Acros, 99.5%), *trans*-stilbene (**3**, Acros, 99%), *cis*-stilbene (**4**, Fluka, ≥95%), 1,1-diphenylethylene (**5**, Acros, 99%), diphenyl (**6**, Fluka, > 98%), decane (Acros, > 99%), *N*-methyl-2-pyrrolidone (NMP, Merck, 99.5%), and sodium acetate trihydrate ($NaOAc \cdot 3H_2O$, Merck, >99.5%) were used as received. The commercial 5 wt % Pd/Al_2O_3 (E40692) catalyst was purchased from Engelhard. The BET surface of the catalyst is 130 $m^2\ g^{-1}$ according to the data sheet provided by the manufacturer. The mean Pd particle size and the corresponding metal dispersion where determined to be 3.3 nm and 0.36, respectively, as described elsewhere.[26]

Catalytic Experiments. All the catalytic experiments were carried out in a specially designed XAS batch cell. The cell possesses two beam paths, which allows probing the liquid phase and the catalyst bed with the solid catalyst separately. The details of this cell are described elsewhere.[25] For a typical experiment, the 5 wt % Pd/Al_2O_3 catalyst (168 mg) was placed in the catalyst bed of the in situ XAS cell, and NMP (1 mL) was carefully added. Then styrene (3.75 mmol, 0.390 g, 0.431 mL) and PhBr (2.5 mmol, 0.393 g, 0.26 mL) followed by a dispersion of $NaOAc \cdot 3H_2O$ (1.1 mmol, 150 mg) in NMP (2 mL) were added to the XAS cell. After setting the desired pressure, the heating was started. The conversion and the yield of the products were followed by GC using a HP 6890 series gas chromatograph equipped with a HP 5 column (30 m × 0.32 mm, i.d. 0.25 μm). Decane was used as internal standard for these measurements. The products were identified by comparison with authentic samples and GC−MS using a HP 6890 series gas chromatograph equipped with a HP 5-MS column (25 m × 0.20 mm, i.d. 0.33 μm) coupled to a HP 5973 mass spectrometer.

QEXAFS Measurements. The QEXAFS measurements were performed at the SuperXAS beamline at the Swiss Light Source (SLS, Villigen, Switzerland). The ring was operated in top-up mode with 400 mA of 2.4 GeV electrons, which emitted polychromatic radiation in a superbend magnet (2.9 T) with a critical energy of 11.9 keV. The beam was collimated by a Rh-coated mirror and then monochromatized using a channel-cut Si(311) crystal in the QEXAFS monochromator.[27] The crystal was continuously moved in a sinusoidal way with a peak-to-peak amplitude of 0.60° corresponding to an energy range of about 1.7 keV at the Pd K-edge at 24.35 keV (see ref 28, Figure 2, right side, fourth black line from the bottom). A rotation speed of 1 Hz was chosen, yielding one EXAFS spectrum each 500 ms. Another Rh-coated mirror behind the QEXAFS monochromator was used to focus the beam on the sample. The samples were measured in transmission mode with a 15-cm ionization chamber filled with Ar in front of the sample and another 15-cm ionization chamber filled with Kr behind the sample. A third 30-cm ionization chamber filled with Ar was used to measure a Pd metal foil located between the second and a third chamber to obtain an absolute calibration value for the energy scale of each spectrum. This value was related to the relative position of the monochromator crystal which was measured simultaneously to each data point with a fast optical angular encoder system, yielding an accurate energy scale for the time-resolved spectra.[29] The ionization chambers were operated with a high voltage of 1.5 kV, and the signals were amplified with Keithley 428 current amplifiers and then measured with a Keithley KUSB3116 data acquisition board using a fast data acquisition software.[30] The acquired data were processed mostly with homemade software, which is partly based on the IFEFFIT package.[31] All EXAFS fits were performed using IFEFFIT, and the according path generation used FEFF6.[32] The spectra from the bottom window of the cell were treated with IFEFFIT algorithms concerning pre-edge and postedge fitting, normalizing, background fitting with AUTOBK and Fourier transformation (FT). For the FT with E_0 = 24355 eV, a *k*-range of 0−14 $Å^{-1}$, a k^3-weighting, and a Kaiser−Bessel window (dk = 0.2 $Å^{-1}$) were chosen. The EXAFS fits of these spectra were all performed within an *R*-range of 1−3 Å, except for the third Pd shell, which was fitted within 4.2−4.8 Å. The

dx.doi.org/10.1021/ja108636u |*J. Am. Chem. Soc.* 2011, 133, 3921–3930

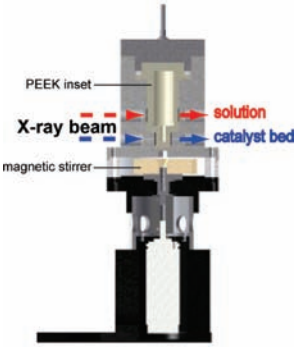

Figure 1. Schematic design of the reactor used for the QEXAFS in situ study. The two beam paths allow separate monitoring of the supported catalyst in the catalyst bed (lower window) and soluble species in the liquid phase (upper window).

principal component analysis (PCA)[33,34] as well as the data treatment for the spectra with very small edge jumps measured in the upper window of the reaction cell were carried out with WinXAS.[35] Here, the AUTOBK algorithm did not yield reasonable results so that cubic spline functions were applied for background fitting. The resulting $\chi(k)$ spectra were Fourier transformed as described above. However, because of the lower Pd concentration, a k-range of $2-10$ Å^{-1} was chosen. EXAFS data fitting was again performed within an R-range of $1-3$ Å. A Pd metal foil was fitted with each of the described data treatments yielding S_0^2 values, which were used as reference to determine the coordination numbers. The linear combination fits (LCF) were also carried out with homemade scripts using the IFEFFIT code. For the fits a range of 24335−24385 eV was chosen to cover the XANES region and thus to get results complementary to the EXAFS fits.

Electron Microscopy Measurements. STEM and EDXS investigations were performed on a field emission transmission electron microscope *Tecnai 30F* (FEI; SuperTwin lens with C_s = 1.2 mm), operated at 300 kV. For the STEM measurements, the spent Pd/Al_2O_3 catalyst was washed with water and dichloromethane to remove inorganic and organic compounds, especially bromides, which could disturb the STEM measurements substantially. For the STEM investigations of the liquid reaction phase, some droplets of the reaction mixture were deposited on a holey carbon foil supported on a copper grid.

RESULTS

First, the in situ cell was optimized with respect to the catalytic and spectroscopic conditions in order to get spectra with a sufficient signal-to-noise ratio. The principle of the cell is shown in Figure 1. The lower beam allows monitoring of the supported catalyst, whereas the upper one with a longer path length permits monitoring the liquid phase. In order to exclude reactions catalyzed by the in situ cell made from stainless steel, a PEEK inset was used. In a preliminary test, the reactor was filled with phenyl bromide (PhBr, **1**), styrene (**2**), and 7 mL of *N*-methyl-2-pyrrolidone (NMP) under Ar. The corresponding measurement through the liquid phase revealed the presence of Pd in the liquid phase. However, the edge jump was rather small, and the quality of the corresponding X-ray absorption spectra was not sufficient for a detailed EXAFS analysis. Reduction of the solvent volume from 7 to 3 mL led to better results. To further increase the amount of leached Pd, Ar was replaced by air in accordance to earlier reports,[36] that led to a higher Pd leaching and subsequent increase in the quality of the EXAFS spectra. The Pd concentration in the liquid phase was determined by comparison of the

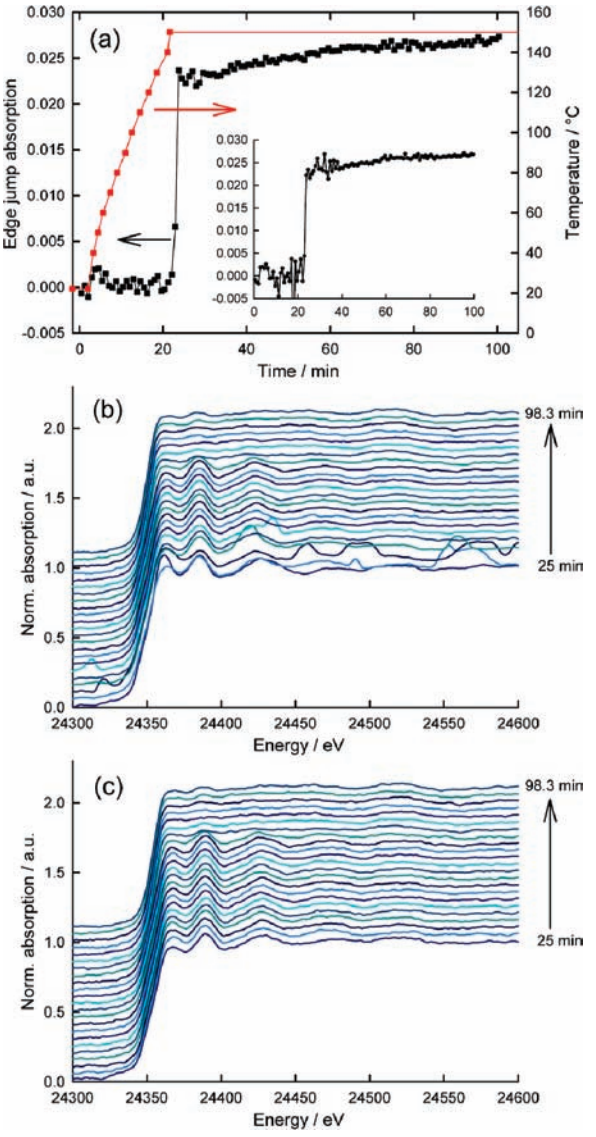

Figure 2. Development of the Pd K-edge absorption in the liquid phase, depending on the temperature and time (a) (the inset shows the results without applying the new median/averaging filter), and the corresponding time-dependent EXAFS spectra of the liquid phase after the stabilization of the edge jump without (b) and with a moving median filter (c).

edge jump with those of reference samples with well-defined concentrations.

At the end of the reaction, the maximum Pd concentration in the liquid phase was determined to be 2.8 mM which equates to a $Pd_{liquid\ phase}$/substrate ratio of 0.3 mol %. This corresponds to 14% of the total amount of Pd in the system. Compared to other catalysts, the Pd leaching in our system is within the typical range.[11,37,38] Conversion and product yields that could be obtained in the in situ experiments were also in the same range as those reported in the literature under comparable reaction conditions (vide infra). For all further experiments, we applied these optimized reaction conditions. In a first step, the leaching of Pd into the liquid phase was investigated by following the development of the Pd K-edge in the liquid phase (upper window). The results are shown in Figure 2. At RT, no Pd was observed in the liquid phase. Also during the heating phase from

RT to 150 °C, no edge jump was visible, indicating that no Pd had yet been leached from the Pd/Al_2O_3 catalyst into the liquid phase. The absence of any edge jump in this stage of the experiments demonstrates that the heterogeneous catalyst remains in the catalyst bed and is not transported into the upper part of the reactor where the liquid phase is probed. We can therefore conclude that all the Pd detected in the liquid phase is actually *leached* Pd. At a reaction temperature of 150 °C, the sudden appearance of an edge jump at the Pd K-edge energy in the liquid phase indicates the formation of leached Pd species from the Pd/Al_2O_3 catalyst: after 22 min of total reaction time, the absorption increases to a significant level within one minute. Thereafter, only a weak ascent of the edge jump is observable up to 60 min reaction time before it maintains a constant level during the remaining reaction time, indicating a constant Pd concentration in the liquid phase (Figure 2a). The corresponding normalized EXAFS spectra are shown in b and c of Figure 2.

In order to get a reasonable quality of the spectra, 400 individual spectra were averaged, which corresponds to a time resolution of 3.3 min for the shown EXAFS spectra, while 100 spectra (time resolution: 50 s) were averaged to determine the edge jump. The EXAFS spectra acquired during the initial increase of the Pd concentration in the liquid phase were rather distorted because of possible superheating of the liquid phase. After another ~20 min, the whole system was equilibrated, and the spectra became clearer (Figure 2b). Since the distortions are randomly distributed over the spectra, a new software tool for QEXAFS data analysis with an implemented median filter was designed to exploit the high time resolution here. The software tool compares every absorption value in each spectrum with the equivalent absorption values of the (in this case) next two neighboring spectra. If the value is the smallest or highest of the resulting three values, it is sorted out as runaway value and replaced by the mean value, which is then considered for further averaging. Thus, runaway values are effectively suppressed as shown in Figure 2c where the distorted spectra are significantly improved so that now all spectra during the active phase of the catalyst can be considered for further data analysis. In addition, the edge jump shown in Figure 2a was determined with filtered spectra, while the results deduced from the unfiltered data are shown in the inset for comparison. This simple example clearly demonstrates the capabilities of this filter to suppress nonstatistical noise, and to our knowledge, it is a novel approach to exploit the high time resolution of QEXAFS data in catalysis and chemical applications in general. One can easily imagine that it is not only effective for heterogeneous solids or inhomogeneous liquid solutions where such time-dependent inhomogeneities occur, but also cancels out randomly appearing electrical disturbances that might show up in the spectra. Prerequisites are a high time resolution compared to the investigated processes and a reproducible and exact data acquisition system.

The first spectrum shown in Figure 2c is measured directly after the huge change of the edge jump described above, after a reaction time around 25 min. It shows clear EXAFS features, and the XANES region, more specifically the exact energy of the Pd K-edge, indicates that the Pd is in a reduced metallic state. During the next 50 min, the spectra look rather similar, indicating that no substantial structural changes occur. Thereafter, the EXAFS spectra show a unique behavior. After ~75 min reaction time, the XANES features disappear almost immediately, whereas the EXAFS region still remains structured. However, the absorption at the edge does not change, indicating that there was no change

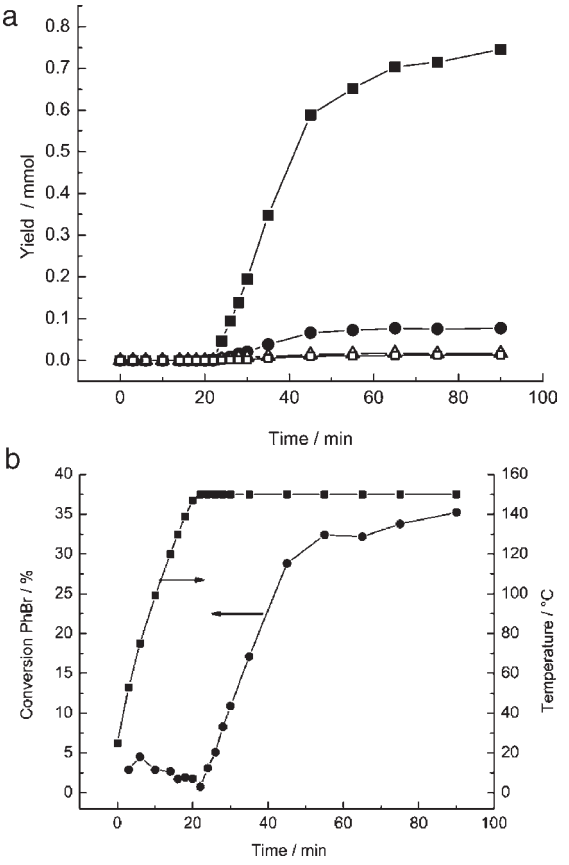

Figure 3. (a) Yield of the main product *trans*-stilbene (**3**, ■) and the observed side products *cis*-stilbene (**4**, ●), 1,1-diphenylethylene (**5**, Δ), and diphenyl (**6**, □) over time as measured by GC. (b) Conversion of PhBr (**1**, ●) over time depending on the reaction temperature (■).

in the Pd concentration in the liquid phase. Therefore, it is most likely that rather structural changes of the leached Pd took place. To ensure that the actually measured Pd in the liquid phase is not just Pd deposited on the reactor wall, the empty PEEK inset was measured after the reaction. No edge jump was observed in this case, demonstrating that no significant amount of Pd was deposited on the inset wall during the reaction and the measured Pd is dissolved in the liquid phase.

The corresponding yields of the formed products as determined by gas chromatography (GC) are shown in Figure 3a. The main product is *trans*-stilbene (**3**), the formation of which is accompanied by the usual side products, *cis*-stilbene (**4**), 1,1-diphenylethylene (**5**), and diphenyl (**6**) (Scheme 1). The formation of benzene was not observed under the applied reaction conditions. The maximum conversion was determined by the amount of the added base. After 90 min, a conversion of 85% relative to the base was achieved. The overall chemoselectivity for the main product **3** was determined to be 89% at the end of the reaction. For comparison, the conversion of PhBr (**1**) was measured, too (Figure 3b). It followed the formation of the products and reached a value of 35% at the end of the reaction.

If one compares the behavior of the edge jump and the EXAFS spectra over time with the catalytic activity, one can observe a good agreement between the conversion of PhBr, the formation of the products, and the structural changes in the EXAFS spectra. Emerging from Figure 3, the conversion of PhBr starts after 22 min. This is exactly the moment when leaching of Pd is indicated

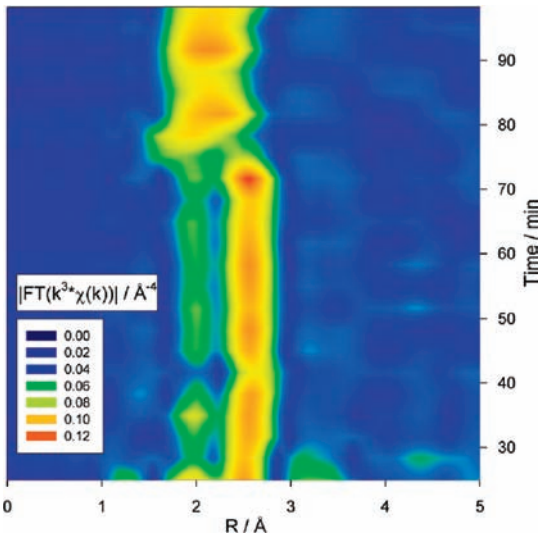

Figure 4. Time-dependent Fourier transformed EXAFS spectra of the liquid phase.

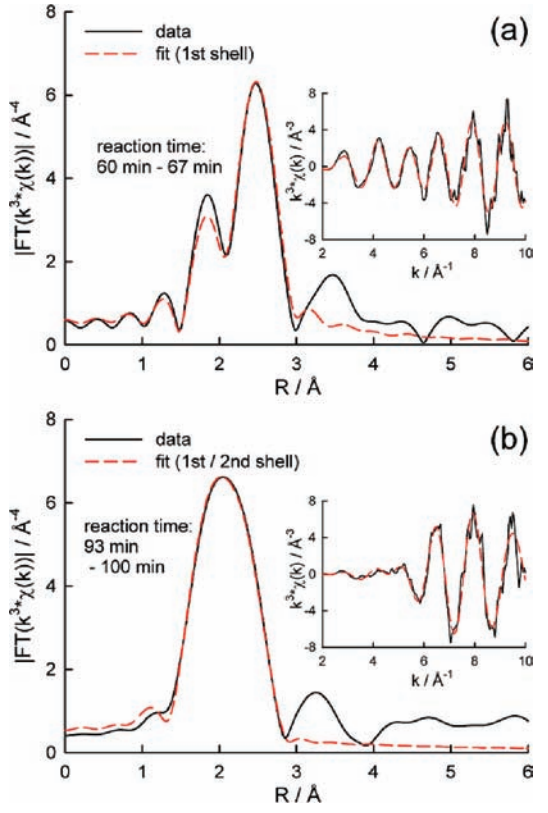

Figure 5. EXAFS refinement fits for (a) active and (b) inactive phase of the catalytic process measured in the liquid phase in *R*- and *k*-space.

by the increasing edge jump (Figure 2a). The conversion then increases quickly at a constant rate until 45 min, and after 75 min, almost no further formation of the reaction products is observed. Interestingly, the decrease in the reaction rate is accompanied by distinct changes in the EXAFS spectra.

In order to get more structural information about the Pd species in the liquid phase and their structural changes, the EXAFS spectra of the liquid phase were Fourier transformed (Figure 4). As one can easily see, there are two well-separated

Table 1. Coordination Numbers (CN) and Interatomic Distances (*R*) Derived from the Analysis of the FT Spectra of the Liquid Phase

reaction stage	shell	CN	$\sigma^2/10^{-3}$ Å^2	*R*/Å
active phase:	Pd	8.7 ± 1.1	10.0 ± 0.9	2.733 ± 0.005
inactive phase:	Br	2.7 ± 0.7	2.6 ± 1.8	2.423 ± 0.019
	Pd	2.2 ± 1.2	5.4 ± 3.6	2.792 ± 0.028

signals with a constant intensity at 1.8 and 2.5 Å during the active phase up to about 75 min and one broad signal at 2.0 Å when the system becomes inactive. The double feature during the active phase could unambiguously be attributed to a single Pd neighbor. This was rationalized by the facts that: (i) the amplitude ratio of the two signals does not change with different *k*-weights as would be expected for contributions of lighter backscattering atoms, (ii) the signals can be reproduced by an EXAFS refinement using the first Pd shell of bulk Pd, and (iii) the signals appear as well in the EXAFS spectra of pure Pd metal foils if the *k*-range used for the Fourier transformation is small, namely below 10−12 Å^{-1} for the upper *k*-limit depending on the chosen E_0. Similar peak doublets for a single coordination caused by the resonating (peaked) behavior of the photoelectron backscattering amplitude were also observed, for example in the case of Ag.[39,40] Thus, the Fourier transformed spectra of the active phase were fitted with a simple model of bulk Pd. For this purpose, 800 individual spectra were averaged to increase the data quality and thus to get as good fit results as possible. Since the observed active and inactive states of the catalyst are stable over a long time interval (Figure 2c), the application of such an extensive averaging is justified here. Consequently, the obtained fit results display a reasonable agreement with the experimental data (Figure 5a). The corresponding values for the coordination numbers and interatomic distances are shown in Table 1.

On the basis of these fit results, one can conclude that most of the leached Pd is present in the form of small Pd colloids with average sizes of about 2 nm during the active phase. This can be deduced from the coordination number of the first shell using the diagrams for fcc lattice structures calculated by Jentys[41] and STEM investigations of the liquid phase, where Pd particles were detected as well (Figure S1, Supporting Information). After the reaction rate decreased significantly, the FT EXAFS spectra of the liquid phase changed in favor of the broad backscattering signal at 2.0 Å (Figure 4). Attempts to fit this peak with a single Pd, O, or Br shell utterly failed. However, the structure can be well reproduced with a combination of a Br and a Pd shell as shown in Figure 5b. For this fit, the first Pd−Pd scattering path of bulk Pd was used in combination with the first Pd−Br shell of tetrabromo-palladate as determined by Makitova et al.[42] The fit results lead to nearly the same Pd−Pd distance as for the small Pd colloids but with a substantially lower coordination number of about 2.2 (Table 1). In relation to pure Pd, this would correspond to about 20% bulk Pd or in relation to the colloids in the active phase to about 30% Pd particles. The Pd−Br distance agrees well with the expected value for $[PdBr_4]^{2-}$ and even better with the first Pd−Br path of $[Pd_2Br_6]^{2-}$, which might also be involved here. The coordination number of about 2.7 corresponds roughly to about 70% of $[PdBr_4]^{2-}$/$[Pd_2Br_6]^{2-}$ species. Thus, at this stage of the reaction, a mixture of about 20−30% Pd colloids and accordingly 80−70% Pd−Br complexes ($[PdBr_4]^{2-}$, $[Pd_2Br_6]^{2-}$) are consistent with the measured EXAFS signal. This superposition of Pd-containing species

dx.doi.org/10.1021/ja108636u |*J. Am. Chem. Soc.* 2011, 133, 3921–3930

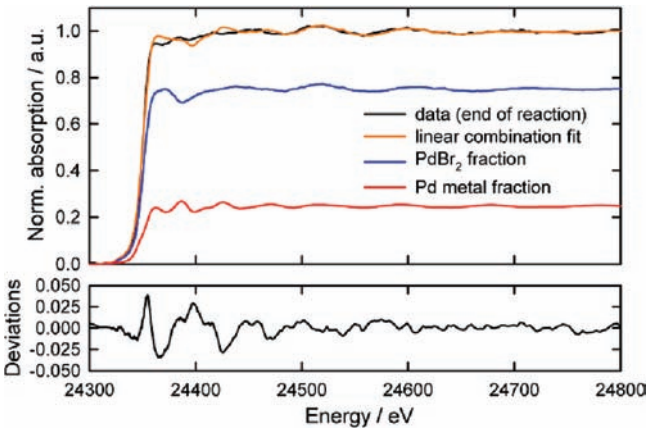

Figure 6. Linear combination fit of spectra of the liquid phase at the end of the reaction using Pd K-edge spectra of a pure Pd metal foil and solid crystalline $PdBr_2$ as references.

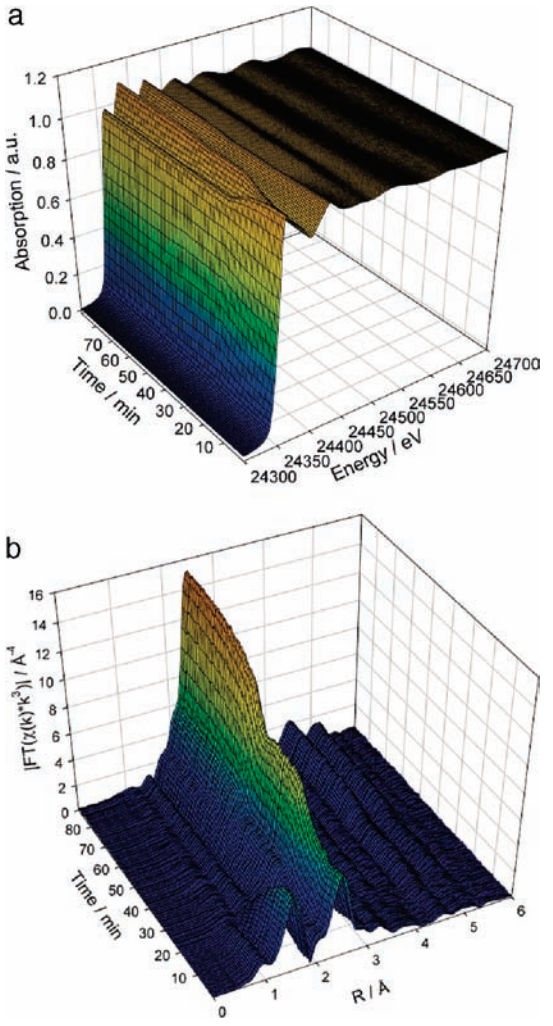

Figure 7. (a) Normalized EXAFS spectra of the 5 wt % Pd/Al_2O_3 catalyst as a function of time. (b) Fourier transformed EXAFS spectra of the 5 wt % Pd/Al_2O_3 catalyst as a function of time.

may also explain the vanishing XANES structure (in particular the two features between 24360 and 24390 eV), which would not be explainable with the presence of only one single species. It is

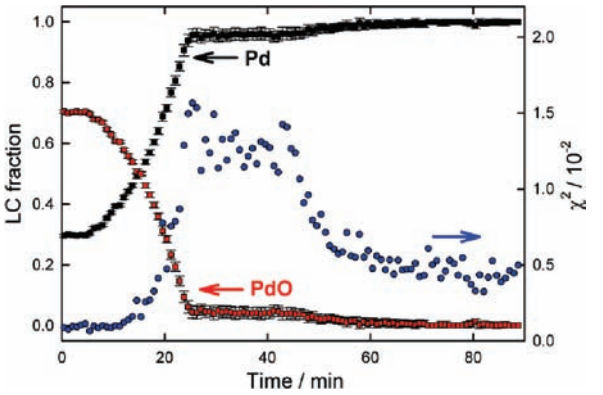

Figure 8. Results of linear combination fits using Pd K-edge spectra of pure Pd metal and PdO and the related fit errors of all spectra at the catalyst bed (bottom part of the in situ cell) as a function of time.

also interesting to see that the mean-square-displacement σ^2 of the Pd−Pd backscattering path is lower during the inactive phase. Although the uncertainties for this value are comparably high, this might be a hint that the Pd colloids might be substantially larger at this point of the reaction compared to the beginning of the leaching process. This is in accordance with the observed Pd-particle growth of the solid catalyst (vide infra).

These results deduced from the above analysis of the Fourier transformed EXAFS spectra could be confirmed by an alternative approach. For this purpose, the corresponding normalized EXAFS spectrum of the solution at the end of the reaction was fitted by a linear combination using the spectrum of pure Pd metal and the spectrum of solid crystalline $PdBr_2$. It yielded 25% Pd metal content versus 75% $PdBr_2$, which is in the same order of magnitude as determined above (Figure 6). The structure of the XANES region is qualitatively reproduced well. The deviations may be attributed to the structural differences between the crystalline $PdBr_2$ and the presumably dissolved bromo-palladates. However, it is obvious that the measured XANES spectra can be reproduced only with mixtures of Pd metal/colloids and bromo-palladates.

The special design of the cell made it also possible to monitor the changes of the solid 5 wt % Pd/Al_2O_3 catalyst during the reaction by probing the lower window of the reactor. The corresponding EXAFS spectra are shown in Figure 7a. Because of the high Pd content in the catalyst bed, time resolutions up to 500 ms for each spectrum are feasible with the acquired data. However, since no changes in the structure of the corresponding EXAFS spectra were detected within less than one minute, the data quality for an optimized EXAFS analysis could be improved by averaging 100 spectra (time resolution: 50 s) without losing any information about the comparable slow dynamics of the system.

At the beginning of the reaction, the catalyst is in a partly oxidized state as indicated by the strong whiteline at about 24350 eV. A linear combination fit using the spectra of metallic Pd and PdO as references in the XANES region of 24335−24385 eV revealed an initial fraction of about 70% PdO and only about 30% metallic Pd (Figure 8). This is reasonable, as the catalyst was stored under air and used without any pretreatment.[16] During the heating phase from RT to 150 °C, the 5 wt % Pd/Al_2O_3 catalyst was reduced as indicated by the continuously decreasing intensity of the whiteline in the EXAFS spectra. The reduction of the catalyst was also evidenced by linear combination fits, which

dx.doi.org/10.1021/ja108636u |*J. Am. Chem. Soc.* 2011, 133, 3921–3930

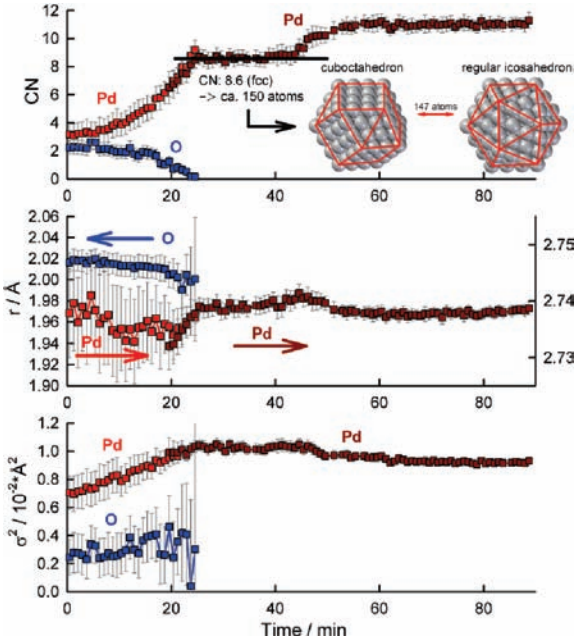

Figure 9. EXAFS refinement fit results for all spectra at the catalyst bed (bottom part) as a function of time. The first region was fitted with a Pd and an O shell, while only the first Pd shell of Pd metal was considered for the second region (displayed in dark red). In the inset, structural models for small Pd clusters are displayed (see text for more details).

revealed a decrease of the PdO amount to about 5% after 25 min and to 0% after 50 min. However, the results of the linear combination fit have to be interpreted carefully because of the increasing fit error after 15 min reaction time (Figure 8). On the basis of the EXAFS results (vide infra), the higher fit error can be assigned to the small size of the Pd particles (~2 nm), leading to less enhanced EXAFS features which are reproduced better by a linear combination fit with a low amount of PdO. Thus, one could expect the catalyst to be already completely reduced after 25 min. The analysis of the Fourier transformed EXAFS spectra of the solid catalyst at the beginning of the reaction reveals two signals at distances of 1.55 Å and 2.45 Å as shown in Figure 7b. The signal at 1.55 Å can be assigned to an oxygen neighbor, and the one at 2.45 Å, to neighboring Pd atoms. The signal at 1.55 Å decreases in intensity during the heating phase and vanishes after 25 min, which coincides with reaching the reaction temperature of 150 °C. The signal at 2.45 Å gains in intensity during the heating period and then reaches a plateau for another 18 min before it increases again after 43 (= 25 + 18) min. The decrease of the signal at 1.55 Å and simultaneous increase of the signal at 2.45 Å are in good agreement with the reduction of PdO to Pd as it was already suggested on the basis of the results from linear combination fit and the decreasing whiteline in the absorption spectra. For a more quantitative analysis we fitted the spectra during the first 25 min with a refinement of the first two calculated scattering paths of PdO using the lattice structure as determined by Waser.[43] It is evident that the behavior of the determined coordination numbers of Pd and O in this period is consistent with the assumed reduction process of Pd (Figure 9). Whereas the coordination number for Pd increases over time from 3 to 8, that of oxygen decreases in the same time interval from 2 to zero. This yields a Pd/O ratio for the initial state of 1.5 which agrees well—within the typical EXAFS errors—with the

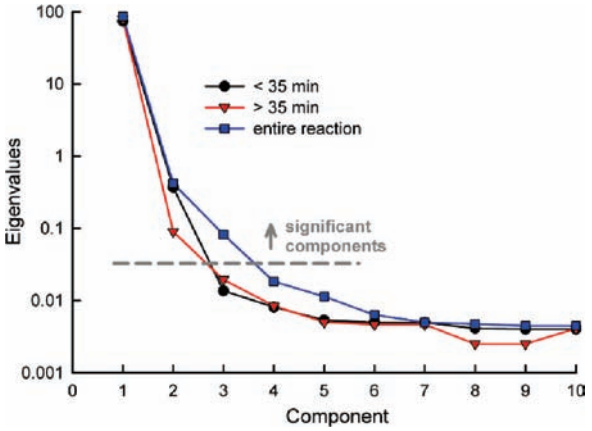

Figure 10. Results of the PCA with normalized EXAFS spectra of the catalyst bed (bottom part) for different time regions and the entire reaction.

linear combination fit results since 70% PdO and 30% Pd correspond to a Pd/O ratio of 1.4.

The mean-square-displacement σ^2 of the Pd−Pd scattering path increases linearly as it could be expected because of the applied temperature ramp, while the one for Pd−O is difficult to investigate properly as the decreasing amount of oxygen leads to increasing fit errors. The distance between Pd and O coincides perfectly with the one found in the literature for PdO.[43,44] The Pd−Pd distance is very close to the literature value of 2.75 Å for pure Pd metal[45] and slightly below the one known for PdO. These deviations are within the expected limits and can be attributed to the small size of the investigated particles. To make sure that there is no unexpected or unexplained additional intermediate state during the first 35 min of the reaction, we applied principal component analysis (PCA) to the normalized EXAFS spectra of this time section as shown in Figure 10. The results suggest only two components, which coincides with the model of a straight reduction process from PdO to metallic Pd.

After this initial reduction of the catalyst, only the first shell of bulk Pd was used as a fit model for the remaining spectra since oxygen content could not be detected any longer. The results are shown in Figure 9 (dark red quadrangles). They are consistent with the fit results for the first 25 min as it can be seen from the 5 min overlap region of the two fits (Figure 9). Apart from the fit model, the same data pretreatment and fit parameters were chosen as for the first 25 min in order to maintain consistency of the results. During the observed plateau after 25 min, the average number of atoms in the Pd particles was derived from the EXAFS first shell data presented in Figure 9 and amounts to about 150 atoms using the theoretically calculated diagrams provided by Jentys.[41,46,47] Interestingly, this value is close to the magic number of 147 atoms, which would be the exact number for a cuboctahedron or a regular icosahedron with four atoms in each edge as has been shown by Mackay.[48] Both geometries are visualized in Figure 9. Fitting the coordination number of the third Pd shell in combination with the first shell is an appropriate way to investigate the particle shape as was also explained by Jentys.[41] Applying this for the spectra acquired during the plateau, a value of ~13.6 is obtained for the coordination number of the third shell (Figure S3, Supporting Information) leading to a N_3/N_1 ratio of about 1.6 ± 0.3. This further supports a spherical shape of the Pd particles consisting of about 150 atoms and supports the conclusion derived from the

dx.doi.org/10.1021/ja108636u | J. Am. Chem. Soc. 2011, 133, 3921–3930

analysis of N_1 for the presence of cuboctahedral or regular icosahedral particles. Thus, we suggest that these kinds of particles with a size of ~2 nm in diameter are the predominant Pd-containing species at this stage of the reaction. This is also in perfect agreement with the scanning transmission electron microscopic (STEM) picture of the solid catalyst ex situ reduced in flowing hydrogen where particles between 2−3 nm were observed.[26]

After this plateau, or after 43 min, respectively, the signal at 2.45 Å starts to increase again. Since the Fourier transformed spectrum does not indicate the formation of a new species, this increase was attributed to particle growth. Extensive fitting of the EXAFS data indeed revealed a particle growth to average sizes far above 5 nm, which constitutes the upper limit for accurate particle-size investigations with EXAFS and is clearly exceeded here. On the other hand, the determined coordination numbers are still below the value of 12 for bulk Pd, showing that metallic Pd is still partly present in small particles at the end of the reaction. The mean-square-displacement σ^2 of the Pd−Pd path decreases because of the higher lattice order that goes along with the particle growth. Only slight changes in the Pd−Pd distance are observable, as expected, since there is no reason for a significant change here. STEM pictures taken of the catalyst at the end of the reaction confirm the suggested growth of the Pd particles (Figure S2, Supporting Information). However, the growth seems to be quite inhomogeneous. Besides particles with a diameter of about 5−8 nm, also bigger particles with diameters of more than 20 nm can be found, which is consistent with the EXAFS results. Again, to exclude the possibility that other processes than particle growth caused the changes in the EXAFS spectra, a PCA was applied to the normalized spectra of the time range from 35 min to the end of the reaction (Figure 10). Since only two components were detected, the second one being rather small, one can assume that the particle growth is indeed the main process occurring in this stage of the reaction.

DISCUSSION

The lively discussion about the active palladium species in Heck reactions[7,8,38] evidence the actual difficulty of its determination and identification in Heck and related C−C coupling reactions due to the inhomogeneous reaction mixture and the low concentration of Pd species in solution. The present study shows that X-ray absorption spectroscopy in terms of XANES and EXAFS combined with a specially designed in situ cell is a powerful tool for in situ investigation in complex matrices like industrially relevant reaction mixtures. The application of QEXAFS with fast single measurements for catching short intermediates and eliminating time-dependent inhomogeneities during the course of the reaction provides additional insight into the reaction mechanism.

The currently dominating opinion in the literature for high-temperature Heck reactions considers the active species in the heterogeneous Heck coupling to be a homogeneous complex, which forms upon leaching from in situ formed colloids (produced from a homogeneous precursor like $Pd(OAc)_2$ or from a supported Pd catalyst).[7,8,11,37] In the course of the reaction, the interaction of the aryl halide with the catalyst surface causes leaching of Pd into the liquid phase and the generation of phenyl-bromo-palladate as the active homogeneous catalyst.[49−51] The leaching ability of PhBr was confirmed by a control experiment under typical reaction conditions with

Scheme 2. Schematic Representation of the Catalytic Cycle of the Heck Reaction with Two Different Reaction Pathways, A and B

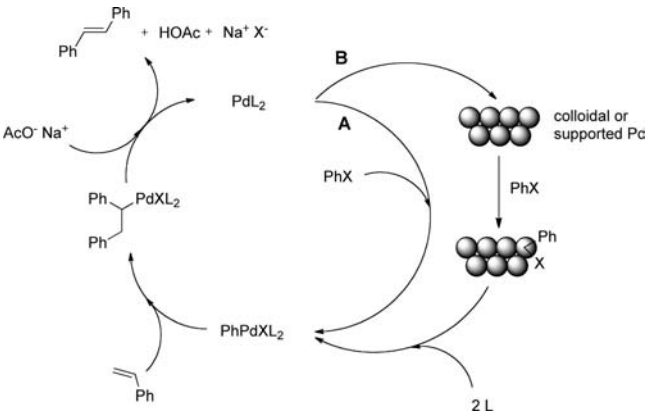

PhBr in NMP, which showed the same leaching behavior for Pd and the original reaction mixture (Figure S4, Supporting Information). One could expect NMP to promote the leaching by stabilizing the leached Pd^{II} species. The catalytic cycle then continues according to the well-known homogeneous mechanism via the coordination of an olefin to the Pd^{II} center, followed by olefin insertion and β-hydride-abstraction (Scheme 2, cycle A).[5,7] Since at the end of the catalytic cycle the Pd is coordinatively undersaturated, it is prone to aggregation and consecutive formation of Pd clusters as well as, depending on the reaction conditions, Pd black.[7,12] It has been speculated that the in situ formation of colloids depends on the activity toward the oxidative addition of the aryl halide applied in the reaction. If the latter is high enough, the formation of colloids is prevented as it is the case for PhI, the most active aryl halide in the Heck reaction (Scheme 2, cycle A). However, when the less active PhBr is used, it was speculated that the slower oxidative addition of PhBr to the underligated Pd^0 species favors the formation of Pd colloids. Therefore one can also propose an alternative cycle where the present Pd colloids do not only serve as Pd reservoir but are directly involved in the catalytic cycle (Scheme 2, cycle B).[52,53] In this case, the formation of the active catalyst is part of the catalytic cycle, since the active catalyst is reduced to colloids at the end of each catalytic cycle and has to be reformed at the beginning of a new catalytic cycle by the interaction of PhBr with the surface of the Pd colloids.

Our results show that during the active phase of the catalysis, mainly Pd colloids are observed, and therefore support that the second cycle B may significantly contribute to the product formation. As the conversion was limited by the amount of the added base, PhBr and styrene were always present in huge excess in the reaction mixture. The fact that the amount of homogeneous Pd complexes increased after 75 min, when the reaction is almost stopped, and became observable by EXAFS with decreasing reaction rate, indicates that indeed the leaching and the subsequent formation of homogeneous Pd species are quite efficient under the applied reaction conditions. Therefore, one can assume that leaching also takes part during the active phase of the reaction. The hypothesized presence of homogeneous species during the active phase of the catalyst is further supported by the observed formation of diphenyl, which is formed under the

inclusion of homogeneous Pd^{II} species.[54,55] This agrees well with the literature, attributing the activity of such catalytic systems to in situ formed homogeneous species.[7,8] The fact that only Pd colloids are observed during the active phase of the catalytic reaction implies that in this case − besides the leaching process − an additional process leads to the reformation of Pd colloids and therefore keeps the amount of homogeneous species in the liquid phase below the observable level for EXAFS. Since the formation of observable quantities of homogeneous Pd species just appears when the formation of products fades out, it is reasonable that one of the steps involved in the formation of the product is involved in the formation of the colloids under the given reactions conditions as well. As PhBr and styrene are present in excess, the formation of an olefin complex is still possible. Therefore, it seems reasonable that the base is taking part in the key step initiating the formation of the colloids, since it is involved in the reaction step that leads to the formation of the product. This again supports our assumption made above, that the second catalytic cycle B contributes essentially to the formation of the products under the applied reaction conditions.

Our findings are in good agreement with newer kinetic investigations. Although most of the catalytic steps have been considered to be rate-determining steps in the past years, it is now accepted that in the case of aryl iodides the rate-determining step is the cleavage of the C−H bond.[12] In the case of the aryl bromide, the situation is different. Although it was believed that the oxidative addition of the aryl bromide is the rate-determining step, it was recently shown that in the case of the high-temperature ligandless Heck reactions, actually the dissolution of the Pd from a heterogeneous precursor, i.e., colloidal or supported Pd, is the rate-determining step. The dissolution of Pd from soluble Pd colloids is more efficient and therefore most likely the dominating process.[7] The oxidative addition of PhBr to the Pd precursor itself is fast as well.[53]

This fits well in the picture as it implies that Pd colloids are the dominating species just before the rate-determining steps and therefore are prone to accumulation (Scheme 2, cycle B).

In accordance with earlier hypotheses, the leaching starts as soon as the supported catalyst is entirely reduced, which is speculated to be a prerequisite for the oxidative addition of the aryl halide as it can only take place with Pd^0 species.[11,56] The in situ reduction of the supported Pd catalyst by the reaction mixture was also observed in other cases, the solvent most likely being the reducing agent although it cannot be excluded that other reagents present in the reaction mixture may support the reduction of the catalyst.[16] Nevertheless, this indicates that, in general, the applied reaction conditions also possess some reducing capabilities despite their corrosive character that is due to the presence of PhBr. Therefore, the reaction mixture may promote both the leaching of Pd as well as the in situ formation of Pd colloids. Together with the formation of the product, this will finally determine the rate of the Pd agglomeration and dissolution. Since the composition of the reaction mixture changes over time, these rates will also change depending on the reaction time.

The observed growth of the Pd particles on the solid catalyst illustrates nicely the hypothesized dissolution/redeposition process of Pd at the end of the reaction. As soon as the reaction rate decreases, the concentration of homogeneous Pd species in the solution increases because of the decomposition of the colloids. Consequently, the equilibrium of the dissolution/redeposition process is shifted in favor of the Pd redeposition leading to the observed growth of the particle of the supported Pd catalyst. When the reaction proceeds with a constant rate the particle size remains constant, and no conclusion concerning a dissolution/redeposition process of Pd at this stage of the reaction can be drawn. However it has been found that the presence of a solid catalyst can favor the redeposition of leached Pd.[57] Under the assumption that continuous leaching is occurring (see above) together with the observation, that the Pd concentration in the liquid phase stays constant we suggest at this stage of the reaction besides an equilibrium between the colloids and the leached Pd also an equilibrium between the latter and the supported Pd particles.

CONCLUSIONS

The in situ formation of Pd colloids under the reaction conditions was observed by using a specially designed in situ EXAFS cell and by a novel QEXAFS analysis approach. The use of the QEXAFS technique does not only allow catching intermediate species in the subsecond scale but also to use the huge amount of data generated by the fast data acquisition hardware for eliminating inhomogeneities in the reaction mixture in the course of the reaction. In fact, changes in the concentration and XANES structure of Pd in the solution were occurring within seconds and sometimes minutes and hours. This allowed averaging over several spectra while the intermediate states were equilibrated and allowed for appropriate EXAFS analysis. Random distortions in the spectra that occurred especially during the course of the reaction because of fluctuations in liquid sample systems were successfully eliminated by applying a median filter. Such filter will generally be a very effective way to improve data quality in certain regions with random distortions. This shows that even unknown and much diluted systems can be investigated effectively with QEXAFS, since it is possible to decide afterward how many spectra are used for averaging and thus how much effective acquisition time is used for each spectrum.

The techniques described above made it possible to follow the leaching of Pd from a heterogeneous catalyst in situ. A more in-depth analysis of the in situ spectra of the liquid phase revealed the presence of both Pd colloids and molecular Pd complexes like $[Pd_2Br_6]^{2-}$ or $[PdBr_4]^{2-}$ that were formed from leached Pd in the liquid phase. During the active phase of the catalysis, mainly Pd colloids were observed, whereas after full conversion (relative to the base) the fraction of Pd complexes increased substantially as the colloids are decomposed partly. This implies the following conclusions for the reaction mechanism: (i) the reaction is catalyzed by molecular Pd complexes which are formed in situ, (ii) the rate-determining step of the Heck coupling reaction with PhBr is most likely the dissolution of Pd from soluble Pd colloids and therefore (iii) these colloids are directly involved in the catalytic cycle and do not only serve as a reservoir when nonactivated substrates like PhBr are used (Scheme 2, cycle B).

The special design of the reactor made it also possible to track the changes of the heterogeneous catalyst in the catalyst bed. The analysis of the corresponding XANES spectra showed a reduction of the Pd, indicating the potential reducing capabilities of the reaction mixture. Furthermore, careful fitting of the EXAFS spectra of the catalyst bed allowed following the changes in the Pd particle size. During the active phase of the catalysis, a constant particle size and concentration were observed, most likely indicating a continuous leaching and redeposition process of Pd. The study indicates the high potential of QEXAFS to

elucidate complex reaction dynamics in industrially important reaction mixtures, not only interesting for C−C couplings with other aryl halides but also for related reaction systems.

■ ASSOCIATED CONTENT

Supporting Information. Additional scanning transmission electron microscopy (STEM) images of the supported catalyst after reaction (Figures S1 and S2), the fitting results for the third shell of the supported Pd particles (Figure S3), and the edge jump of the Pd K-edge in the liquid phase after heating to 150 °C when only PhBr (**1**) was present in the reaction mixture (Figure S4). This material is available free of charge via the Internet at http://pubs.acs.org.

■ AUTHOR INFORMATION

Corresponding Authors
grunwaldt@kit.edu; baiker@chem.ethz.ch

■ ACKNOWLEDGMENT

Financial support by the Swiss National Science Foundation is kindly acknowledged. We thank Dr. Maarten Nachtegaal for his assistance during XAS measurements and the SLS at PSI (Switzerland) for providing beam time. Electron microscopy investigations were carried out by Dr. Frank Krumeich at the Electron Microscopy ETH Zurich (EMEZ). Finally, we thank Prof. Klaus Köhler (TU München) for stimulating discussions, especially in the beginning of the study.

■ REFERENCES

(1) Blaser, H.-U.; Indolese, A.; Naud, F.; Nettekoven, U.; Schnyder, A. *Adv. Synth. Catal.* **2004**, *346*, 1583–1598.
(2) Torborg, C.; Beller, M. *Adv. Synth. Catal.* **2009**, *351*, 3027–3043.
(3) Heck, R. F.; Nolley, J. P. *J. Org. Chem.* **1972**, *37*, 2320–2322.
(4) Mizoroki, T.; Mori, K.; Ozaki, A. *Bull. Chem. Soc. Jpn.* **1971**, *44*, 581.
(5) Oestreich, M., Ed. *The Mizoroki-Heck Reaction*; John Wiley & Sons: Chichester, 2009.
(6) Biffis, A.; Zecca, M.; Basato, M. *Eur. J. Inorg. Chem.* **2001**, 1131–1133.
(7) de Vries, J. G. *Dalton Trans.* **2006**, 421–429.
(8) Astruc, D. *Inorg. Chem.* **2007**, *46*, 1884–1894.
(9) Kaneda, K.; Higuchi, M.; Imanaka, T. *J. Mol. Catal.* **1990**, *63*, L33–L36.
(10) Augustine, R. L.; Oleary, S. T. *J. Mol. Catal. A: Chem.* **1995**, *95*, 277–285.
(11) Köhler, K.; Kleist, W.; Pröckl, S. S. *Inorg. Chem.* **2007**, *46*, 1876–1883.
(12) Schmidt, A. F.; Al Halaiqa, A.; Smirnov, V. V. *Synlett* **2006**, 2861–2878.
(13) Kleist, W.; Pröckl, S. S.; Köhler, K. *Catal. Lett.* **2008**, *125*, 197–200.
(14) Michailowski, A.; Grunwaldt, J.-D.; Baiker, A.; Kiebach, R.; Bensch, W.; Patzke, G. R. *Angew. Chem.* **2005**, *44*, 5463.
(15) Evans, J.; O'Neill, L.; Kambhampati, V. L.; Rayner, G.; Turin, S.; Genge, A.; Dent, A. J.; Neisius, T. *J. Chem. Soc., Dalton Trans.* **2002**, 2207–2212.
(16) Reimann, S.; Grunwaldt, J.-D.; Mallat, T.; Baiker, A. *Chem. Eur. J.* **2010**, *16*, 9658–9668.
(17) Ellis, P. J.; S., F. I. J.; Hackett, S. F. J.; Wilson, K.; Lee, A. F. *Angew. Chem., Int. Ed.* **2010**, *49*, 1820–1824.
(18) Aschwanden, L.; Mallat, T.; Grunwaldt, J.-D.; Krumeich, F.; Baiker, A. *J. Mol. Catal. A: Chem.* **2009**, *300*, 111.
(19) Rohr, M.; Grunwaldt, J.-D.; Baiker, A. *J. Mol. Catal. A: Chem.* **2005**, *266*, 253–257.
(20) Frahm, R. *Nucl. Instrum. Methods Phys. Res., Sect. A* **1988**, *270*, 578–581.
(21) Frahm, R. *Rev. Sci. Instrum.* **1989**, *60*, 2515–2518.
(22) Lützenkirchen-Hecht, D.; Grunwaldt, J.-D.; Richwin, M.; Griesebock, B.; Baiker, A.; Frahm, R. *Phys. Scr.* **2005**, *T115*, 831–833.
(23) Grunwaldt, J.-D.; Beier, M.; Kimmerle, B.; Baiker, A.; Nachtegaal, M.; Griesebock, B.; Lützenkirchen-Hecht, D.; Stötzel, J.; Frahm, R. *Phys. Chem. Chem. Phys.* **2009**, *11*, 8779–8789.
(24) Clausen, B. S.; Topsøe, H.; Frahm, R. *Adv. Catal.* **1998**, *42*, 315.
(25) Grunwaldt, J.-D.; Ramin, M.; Rohr, M.; Michailovski, A.; Patzke, G. R.; Baiker, A. *Rev. Sci. Instrum.* **2005**, *76*, 054104.
(26) Reimann, S.; Mallat, T.; Baiker, A. *J. Catal.* **2007**, *252*, 30–38.
(27) Frahm, R.; Richwin, M.; Lützenkirchen-Hecht, D. *Phys. Scr.* **2005**, *T115*, 974–976.
(28) Stötzel, J.; Lützenkirchen-Hecht, D.; Frahm, R. *Rev. Sci. Instrum.* **2010**, *81*, 073109.
(29) Stötzel, J.; Lützenkirchen-Hecht, D.; Fonda, E.; De Oliveira, N.; Briois, V.; Frahm, R. *Rev. Sci. Instrum.* **2008**, 79.
(30) Stötzel, J.; Lützenkirchen-Hecht, D.; Frahm, R. *J. Synchrotron Rad.* **2011**, in print, doi:10.1107/S0909049510051897.
(31) Newville, M. *J. Synchrotron Rad.* **2001**, *8*, 322–324.
(32) Rehr, J. J.; Albers, R. C. *Rev. Mod. Phys.* **2000**, *72*, 621–654.
(33) Malinowski, E. R. *Factor Analysis in Chemistry*, 3rd ed.: Wiley-Interscience: New York, 2002.
(34) Jackson, J. E. *A user's guide to principal components*; John Wiley & Sons: New York, 1991.
(35) Ressler, T. *J. Synchrotron Rad.* **1998**, *5*, 118–122.
(36) Pröckl, S. S.; Kleist, W.; Köhler, K. *Tetrahedron* **2005**, *61*, 9855–9859.
(37) Biffis, A.; Zecca, M.; Basato, M. *J. Mol. Catal. A: Chem.* **2001**, *173*, 249–274.
(38) Phan, N. T. S.; Van Der Sluys, M.; Jones, C. W. *Adv. Synth. Catal.* **2006**, *348*, 609–679.
(39) Dalba, G.; Fornasini, P.; Rocca, F.; Mobilio, S. *Phys. Rev. B* **1990**, *41*, 9668–9675.
(40) Lützenkirchen-Hecht, D.; Strehblow, H.-H. *Surf. Interface Anal.* **2006**, *38*, 686–690.
(41) Jentys, A. *Phys. Chem. Chem. Phys.* **1999**, *1*, 4059–4063.
(42) Makitova, D. D.; Korableva, L. G.; Kraschoka, O. N.; Lavrent'ev, I. P.; Atovmyan, L. O.; Khidekel, M. L. *Koord. Khim.* **1986**, *12*, 1262–1269.
(43) Waser, J.; Levy, H. A.; Peterson, S. W. *Acta Crystallogr.* **1953**, *6*, 661–663.
(44) Grunwaldt, J.-D.; Caravati, M.; Baiker, A. *J. Phys. Chem. B* **2006**, *110*, 9916–9922.
(45) Kittel, C.; McEuen, P. *Introduction to Solid State Physics*; John Wiley & Sons: New York, 2005.
(46) Clausen, B. S.; Nørskov, J. K. *Top. Catal.* **2000**, *10*, 221–230.
(47) Grunwaldt, J.-D.; Molenbroek, A. M.; Topsøe, N. Y.; Topsøe, H.; Clausen, B. S. *J. Catal.* **2000**, *194*, 452–460.
(48) Mackay, A. L. *Acta Crystallogr.* **1962**, *15*, 916–918.
(49) Schmidt, A. F.; Mametova, L. V. *Kinet. Catal.* **1996**, *37*, 406–408.
(50) Reetz, M. T.; Westermann, E. *Angew. Chem., Int. Ed.* **2000**, *39*, 165–168.
(51) Gniewek, A.; Trzeciak, A. M.; Ziolkowski, J. J.; Kepinski, L.; Wrzyszcz, J.; Tylus, W. *J. Catal.* **2005**, *229*, 332–343.
(52) Schmidt, A. F.; Khalaika, A. *Kinet. Catal.* **1996**, *39*, 803–809.
(53) Schmidt, A. F.; Al-Halaiqa, A.; Smirnov, V. V. *Kinet. Catal.* **2007**, *48*, 716–727.
(54) McGuinness, D. S.; Cavell, K. J.; Skelton, B. W.; White, A. H. *Organometallics* **1999**, *18*, 1596–1605.
(55) Schmidt, A. F.; Smirnov, V. V.; Al-Halaiga, A. *Kinet. Catal.* **2007**, *48*, 390–397.
(56) Köhler, K.; Pröckl, S. S.; Kleist, W. *Curr. Org. Chem.* **2006**, *10*, 1585–1601.
(57) Huang, L.; Wong, P. K.; Tan, J.; Ang, T. P.; Wang, Z. *J. Phys. Chem. C* **2009**, *113*, 10120–10130.